Cooperative Agreement # CR-83327701

INVESTIGATING MIXING IN BAFFLED OZONE CONTACTORS USING 3-D LASER-INDUCED FLUORESCENCE AND REACTIVE TRANSPORT MODEL

FINAL REPORT

Prepared by

Jaehong Kim, Ph.D.
Principal Investigator
Georgia Institute of Technology
Assistant Professor of School of Civil & Environmental Engineering
200 Bobby Dodd Way
Atlanta, GA 30332-0373

Philip Roberts, Ph.D., P.E.
Georgia Institute of Technology
Professor of School of Civil & Environmental Engineering
790 Atlantic Drive N.W.
Atlanta, GA 30332-0355

and

Dooil Kim
Georgia Institute of Technology
Graduate Research Assistant of School of Civil & Environmental Engineering
200 Bobby Dodd Way
Atlanta, GA 30332-0373

For

Michael S. Elovitz, Ph.D.
EPA Project Manager

U.S. Environmental Protection Agency
Cincinnati, Ohio 45268

ACKNOWLEDGEMENT

This research was funded by the U. S. Environmental Protection Agency (Cooperative Agreement # CR-83327701). Mention of trade names or commercial products does not constitute endorsement or recommendation for use. The scientific views expressed are solely those of the authors and do not necessarily reflect those of USEPA. Mr. Lon Couillard at Milwaukee Water Works, Milwaukee, WI is thankfully acknowledged for technical support and reviewing the manuscript. The content of the report was submitted to a peer-reviewed journal, *Journal American Water Works Association*, on December 22, 2008.

ABSTRACT

Three-dimensional laser-induced fluorescence (3DLIF) was applied to visualize and quantitatively analyze hydrodynamics and mixing in a multi-chamber ozone contactor, the most widely used design for water disinfection. The results suggested that the mixing was characterized by extensive short-circuiting between chambers, internal recirculation within the chambers, and dead zones at the chamber centers. Due to these non-ideal mixing behaviors, the hydrodynamics in the entire reactor showed greater dispersion than a series of completely mixed reactors. These flow patterns could be diminished by decreasing the channel width, while the impacts of the flow rate and baffle gap were negligible within the range investigated. Accordingly, reactive transport model simulations suggested that the overall reactor performance could be significantly improved by preventing these flow behaviors. The 3DLIF technique developed and presented in this study is expected to provide a novel tool for existing reactor diagnosis and retrofitting as well as for new reactor design.

TABLE OF CONTENT

1. INTRODUCTION

A common reactor design used for ozonation of drinking water is the multi-chamber bubble-diffuser contactor in which one or more of the upstream chambers are equipped with bubble diffusers that transfer ozone gas to the water. The remaining downstream chambers provide additional contact time for residual dissolved ozone to inactivate pathogenic microorganisms. This design is intended to provide consecutive meandering upward and downward flows with relatively low dispersion, the extent of which is commonly quantified by a Péclet number ($Pé = UL/E$, where U = velocity; L = characteristic length; and E = turbulent diffusivity) or dispersion number ($d = 1/Pé$). Higher Péclet numbers (lower dispersion numbers) are characteristic of a reactor closer to an ideal plug-flow reactor (PFR). With respect to regulatory compliance (USEPA, 1991), a higher *Pé* value corresponds to a higher t_{10} to HRT ratio, t_{10} /HRT, where t_{10} is the minimum residence time for 90% of fluid elements and HRT the theoretical hydraulic residence time, and hence a greater disinfection credit. This flow condition also helps minimize the process overdesign (*e.g.*, overestimation of the reactor volume and/or residence time) and reduce the formation of disinfection byproducts such as bromate (Roustan et al., 1993; Do-Quang et al., 2000a; Kim et al., 2007a). However, undesirable flow patterns including short-circuiting (preferential flow through a narrow cross-section of the chamber), internal recirculation within chambers, or backmixing (mixing of chamber effluent with influent) can occur depending on the design and operating conditions. For the ozone contactors designed with the goal of providing the hydrodynamic condition close to that of PFR, it is important to prevent the occurrence of these non-ideal mixing behaviors, as they diminish the overall inactivation efficiency.

Our recently published study (Kim et al., 2007b) investigated mixing in a twelve-chamber ozone bubble-diffuser contactor at the Linnwood Water Plant Ozone Facility (LWPOF) of Milwaukee Water Works, Milwaukee, WI. The results of full-scale tracer tests in a portion of the reactor (from the first to tenth chambers) were modeled using a series of axial dispersion reactors (ADRs) with a very high dispersion number, d = 10,000. This implied that the hydrodynamics in each chamber was very close to that in an ideal continuously stirred tank reactor (CSTR), although detailed mixing condition in each chamber was not experimentally determined. Such a

complete mixing in each chamber was not an expected flow condition for the multi-chamber reactor. Consequently, a subsequent model simulation suggested that designing each chamber closer to the PFR would significantly increase the efficiency of the pathogen inactivation and decrease the formation of bromate at the same time, even though the current operation of this plant met the regulations in both regards.

However, it has been extremely challenging to experimentally determine the actual flow conditions within each chamber of the full-scale ozone contactor. Lack of such knowledge also makes it difficult to develop strategies to modify the flow conditions to approach a plug flow. Conservative tracer tests in conjunction with flow models such as CSTR-in-series model and ADR model are common approaches to investigate mixing in reactors. However, they cannot explain the complex, time-dependent, three-dimensional flows that occur within the chambers, but rather treat the overall reactor as a black box. More sophisticated simulations based on time-averaged computational fluid dynamics (CFD) have been used to predict these flow irregularities within ozone contactors (Henry and Freeman, 1995; Murrer et al, 1995; Huang et al, 2002), but they have not been experimentally verified.

In this study, we apply a novel method using three-dimensional laser-induced fluorescence (3DLIF) (Tian and Roberts, 2003) to visually and quantitatively analyze the hydrodynamics in a multi-chamber ozone contactor. We have recently applied this technique to examine flow in a two-chamber ozone contactor equipped with a side-stream venturi injector for the first time (Kim et al., 2008). In the 3DLIF system, a planar monochromatic laser sheet is projected into the flow field and causes a water soluble fluorescent tracer dye to emit light (Guiraud et al, 1991). Three-dimensional flow pictures are obtained by scanning the laser sheet across the reactor and capturing the fluoresced light by a high speed CCD camera. Using this non-intrusive technique, instantaneous, 3D mixing characteristics in the lab-scale model of the ozone contactor at the LWPOF (*i.e.* which was scaled down by Froude number similitude according to Kim et al. (2008)) were visually and quantitatively examined. 3DLIF was further applied to examine the design and operating factors that affected the mixing in the model ozone contactor.

2. EXPERIMENTAL METHODS

2.1. 3DLIF system

A beam of laser with wavelength of 514 nm and intensity of 1.75 W was generated by an Innova 90 Argon-ion laser (Coherent®, Palo Alto, CA). The laser beam was converted to a vertical laser sheet using a mirror which oscillated very rapidly around a horizontal axis. Another mirror oscillated perpendicular to the first mirror to scan the laser sheet horizontally across the reactor. The laser sheet passed through a plano-convex lens of 250 mm diameter and 940 mm focal length (the distance between the lens and scanning mirrors) so that the laser beam was always parallel to the reactor axis. The laser sheet scanning was synchronized with an image capturing device (Dalsa® CA-D6 high speed CCD camera, Ontario, Canada) and Video Savant® software (IO Industries, Inc., Ontario Canada) to obtain twenty slices of images with 256 gray levels per each scan (completed within 1 s) which were streamed to a high-capacity storage device. A long-pass optical filter with a 530 nm cut-off (Schott Glass 530, Reynard Corporation, San Clemente, CA) was placed between the lens and the CCD sensor to remove scattered incident laser light. The images were then processed pixel-by-pixel to correct for vignetting (darker margins caused by the optical lens characteristics) and attenuation (the loss of laser intensity as it passes through the solutions containing laser absorbing dye) using the software *TFlook* developed by Tian and Roberts (2003). *TFlook* converted the images into files that could be read by *Tecplot*® (Bellevue, WA) for 3D data visualization, analysis, and plotting. The dye concentration was estimated from the pixel intensity in the LIF images using a calibration factor that was obtained by a linear regression of fluorescence intensity of images of standard dye solutions with concentration of 25 and 50 μg/L.

2.2. Model Ozone contactor

A laboratory-scale model of the ozone contactor at the LWPOF was constructed using transparent Lucite® sheets (3M, St. Paul, MN). The LWPOF is equipped with four identical ozone contactors, each consisting of 12 chambers with an overall volume of 128,000 ft^3 (0.957 MG). Details of the design are presented in Kim et al. (2007b). The dimensions and operating

conditions (*e.g.*, the flow rate) for the model were determined from Froude number similitude (Hannoun et al., 1998; Ettema et al, 2000; Kim et al., 2008). The physical variables that determined the dimensions and flow characteristics were reduced to dimensionless terms using the Buckingham π-theorem (Buckingham, 1914; Munson et al, 1998) as follows:

$$\phi\left(\frac{U}{\sqrt{gH}}, \frac{W}{H}, \frac{L}{H}, \frac{tU}{H}\right) = 0 \qquad (1)$$

where $U/\sqrt{gH}$ = Fr (Froude number), U = velocity, g = gravitational acceleration, H = water depth, t = residence time, and φ = pi function. The model reactor was scaled by keeping these dimensionless terms, including *Fr*, the same as the full-scale reactor. The length scale ratio was chosen to be 1:40 to best fit the model reactor to the LIF system (*i.e.* the size of laser plane), and the velocity and time scales were, therefore, $(1/40)^{1/2}$. The configuration and dimensions of the model ozone contactor are shown in Figure 1.

2.3. Tracer Test

Dechlorinated tap water filtered through 10 and 0.1 μm fiber cartridge filters was fed into the model reactor at room temperature (20±2^{o}C) at a flow rate of 12 L/min, which corresponded to 45 MGD in the full-scale contactor (one of the flow rates studied in Kim et al. 2007b). The influent water was evenly distributed over the cross-section of the reactor inlet using a permeable sponge made of horse-hair. After reaching steady-state, 1 mL of 100 mg/L Rhodamine 6G (Sigma-Aldrich, St. Louise, MO) solution was injected as a pulse using a syringe into the inlet pipe. The tracer tests were performed without ozone gas injection so that the tracer was conservative. Images were acquired by the 3DLIF system for 2 to 4 times the theoretical residence time (3.89 min for the flow rate of 12 L/min). Residence time distribution (RTD) curves were obtained by averaging the dye concentrations over the cross-section of the baffle gap (*i.e.* the opening between consecutive chambers at the location closest to the preceding chamber) using *Tecplot*®.

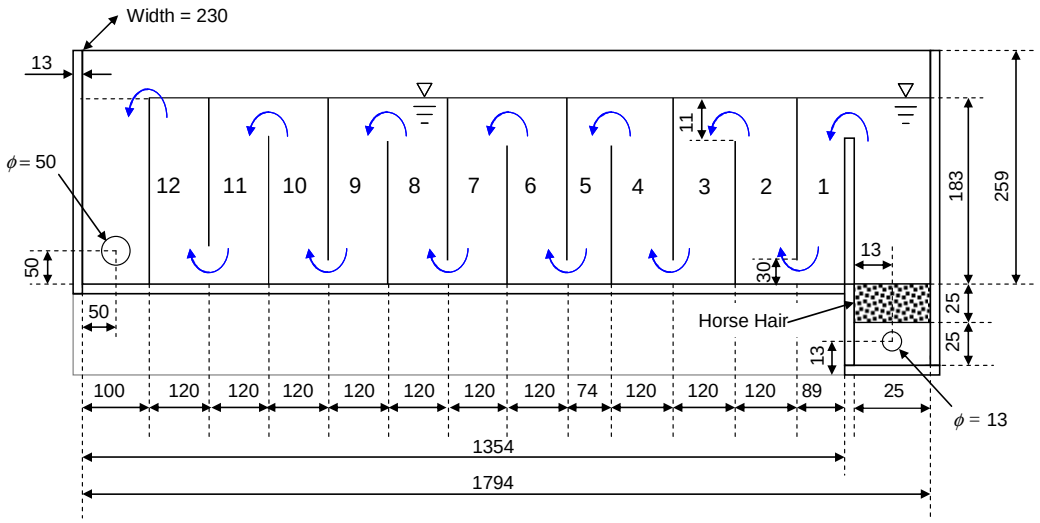

(a)

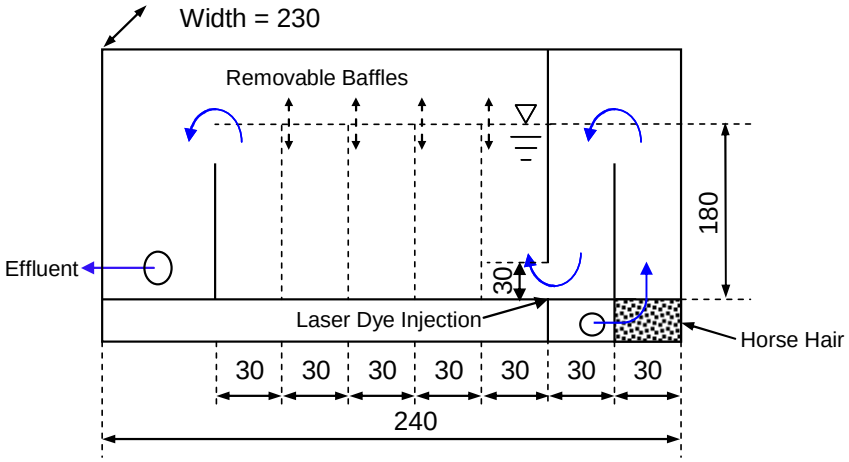

(b)

Figure 1. Schematic diagram of (a) lab-scale replica of the LWPOF ozone contactor and (b) the modified ozone contactor with flexible channel width. (units in mm)

2.4. Reactor Design Alterations

Additional experiments were performing by changing the baffle gap (the distance between the bottom of the underflow baffle and the bottom of the reactor, or between the top of the overflow baffle and water surface) of the model reactor. The gap was adjusted to either a “wide” (twice the

original baseline condition) or “narrow” (half the original baseline condition). A second model reactor was constructed to examine the influence of channel width (the distance between consecutive baffles). This reactor consisted of only two chambers, but the width of the second chamber could be varied at 30, 60, 90, 120, and 150 mm. The channel width of 120 mm corresponded to the original channel width of reactive chambers (the second to fourth chambers and sixth to twelfth chambers) in the model LWPOF reactor. A baffle gap of 30 mm was used for all the experiments. Other experimental conditions for tracer tests and 3DLIF system operation were identical to those used for the model LWPOF reactor except that the flow rate was reduced to half, *i.e*. 6 L/min. The tracer dye was injected at the entrance of the varying-width chamber as a pulse (evenly distributed across the *y*-axis of the chamber).

3. RESULTS AND DISCUSSION

3.1. 3DLIF Analysis

The RTD curves obtained from the 3DLIF experiments (by averaging the dye concentration at the cross-section of the outlet of the tenth chamber) were compared with the RTD curves obtained from the full-scale tracer tests performed by Kim et al. (2007b) for the first to tenth chambers. Flow rates for the model reactor were 6 and 12 L/min, which correspond to 22.5 and 45 MGD in full-scale. The flow rates for the full-scale tracer tests were 22.8 and 42.9 MGD. All the RTD curves shown in Figure 2 were normalized (*i.e*. E_θ = normalized concentration, θ = normalized time, *i.e*. time divided by mean residence time experimentally determined) such that the area under the curve is unity. The RTD curves agreed well, suggesting that the overall flow characteristics of the model and full-scale reactors are very similar even though there was no gas flow in the model reactor. The peaks are slightly lower and the tail parts of RTD curves (*i.e*. after $\theta \cong 1.2$) were slightly raised for the lab-scale RTD. This might have resulted since some dye was trapped in the horse hair sponge that was used to disperse the dye across the reactor inlet or the higher surface area per volume of the model reactor contributed to some retardation in dye transport near the reactor walls. The RTD curves were not affected by the flow rates within the range investigated. A CSTR-in-series model analysis suggests that the overall hydrodynamics of the reactor could be best represented by a series of 7 to 8 CSTRs-in-series. Considering that the

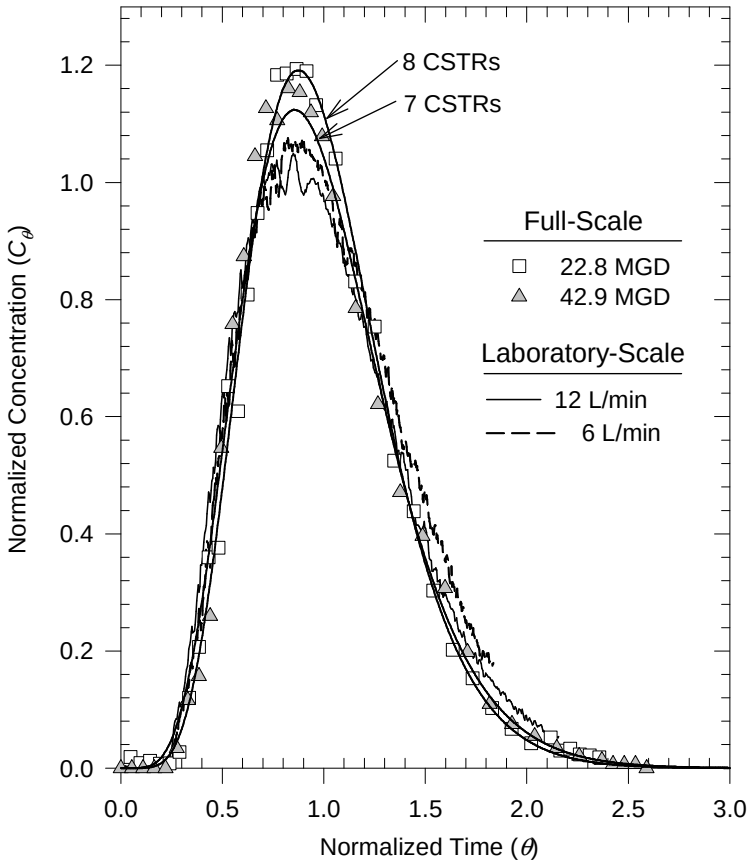

Figure 2. Comparing normalized RTD curves of the LWPOF full-scale ozone contactor and lab-scale model reactor and CSTR-in-series model simulation results.

reactor consisted of 10 chambers, the observed RTD could not be explained solely by this model. The reactor with the theoretical maximum level of dispersion (*i.e.* when each chamber is an ideal CSTR) would be 10 CSTRs-in-series for the reactor with 10 chambers.

Alternatively, the aforementioned non-ideal flow conditions might exit inside each chamber, causing the tracer (and fluid elements) to disperse along the flow direction much more widely than expected for a series of CSTRs. The experimental 3DLIF results shown in Figure 3 provide critical information on flows inside the reactor. This series of images shows dye concentration profiles in the vertical plane facing the camera (*x*-*z* plane) placed in the middle of the chamber (*i.e.* the center of the reactor width along *y*-axis). Note that similar sets of images could be

obtained at different lateral locations along *y*-axis to construct complete 3D images for the flow within the reactor. Since there was little difference in these flow images, however, and because the effect of the reactor walls in the *x*-*z* plane on the flow was negligible, only representative 2D images are presented.

Figure 3 shows the images taken at t = 10 s (corresponding to 1.1 min for the full-scale reactor) to t = 700 s (73.8 min for the full-scale) for the first to tenth chambers. At t = 10 s, the flow instantly reached the opposite wall (the baffle between the first and the second chambers) and was redirected downward along the first chamber. As the tracer entered the second chamber (t = 30 s), it moved rapidly along the wall between the second and third chambers, (*i.e.* short-

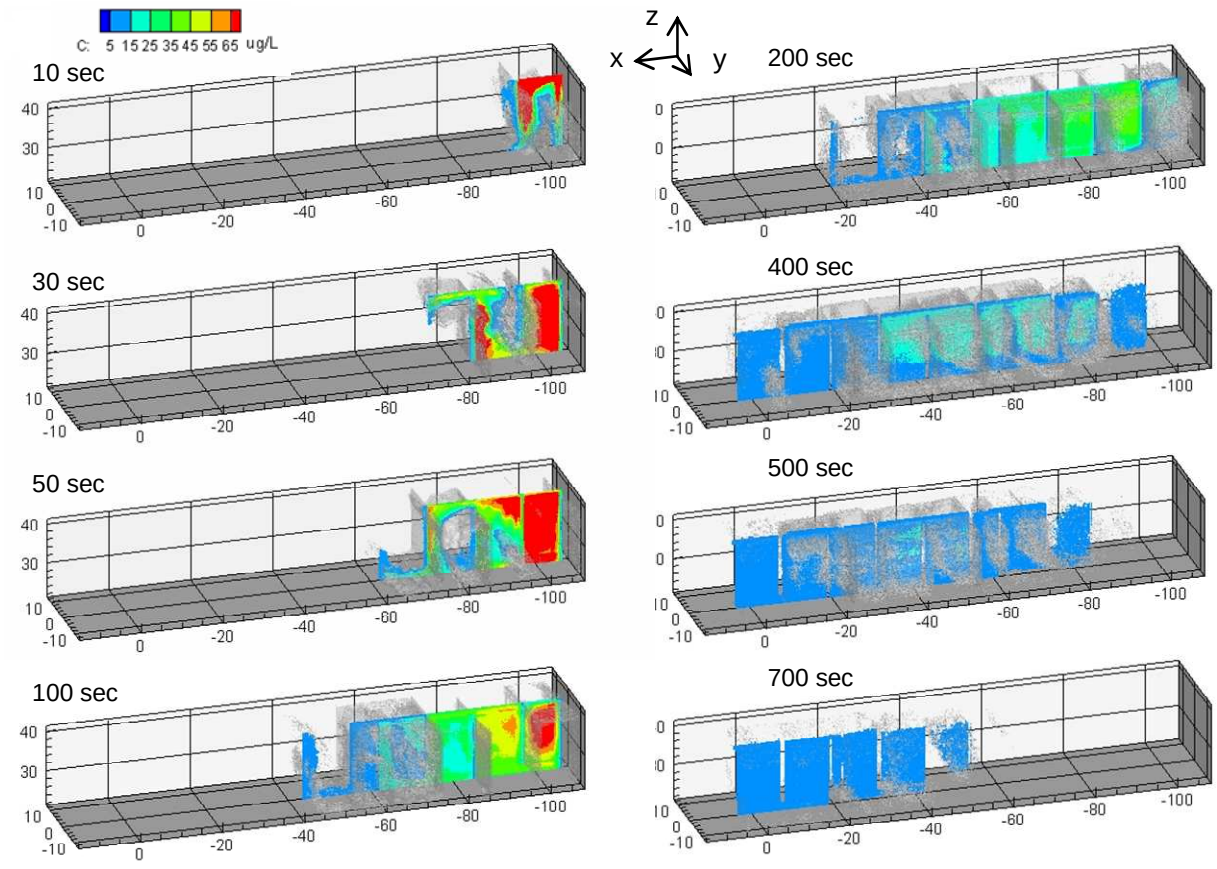

Figure 3. 2D LIF images showing tracer dye transport behavior through the model ozone contactor obtained from 3DLIF experiment.

circuiting). The tracer then split into two, one entering the third chamber and the other returning back to the second chamber. The latter formed an internal recirculation within the second chamber. As a result of this preferential flow formation, a large dead zone formed at the center of each chamber in which mixing was significantly impaired, as is clearly noticeable in the images at t = 50 s (3rd chamber. The tracer then moved into the subsequent chambers and followed the same flow pattern, although it became less visible as the tracer dispersed and its concentration gradually became lower.

Normalized tracer exit curves at each chamber were constructed from the 3DLIF results by averaging the dye concentrations at the cross-section of each chamber outlet, and are shown in Figure 4. Note that independent measurements of tracer concentration at the outlets would be required to obtain similar information from conventional tracer tests. In contrast, a single 3DLIF experiment provides detailed RTD information at any position within the reactor. The RTD curve obtained at the outlet of the first chamber clearly showed short-circuiting (the appearance of a peak much earlier than (measured) mean residence time, or $\theta = 1.0$). The second sharp peak resulted from the internal recirculation (tracer exiting the chamber after the first round of internal recirculation). The RTD curves of the subsequent chambers showed the early peak becoming smaller with a single peak centered at $\theta = 1.0$, suggesting that short-circuiting diminished in each subsequent chamber. This explains why the presence of non-ideal flow characteristics in each chamber were not detected in full-scale tests due to dispersion of the tracer across the entire span of the reactor, and "dilution" of the impact of each chamber flow on the overall reactor flow.

The normalized RTD curves for each chamber in Figure 4 were further analyzed using the CSTRs-in-series model. For each figure, the number of CSTRs was the same as the number of chambers. The RTD curves for the first and second chambers matched well with one CSTR model and two CSTRs-in-series model, respectively, except for the shorter residence time in which short-circuiting peaks appeared. But the model began to deviate beyond third chamber and the discrepancy became greater for downstream chambers. It is noteworthy that the portion of the reactor with more than three chambers had a wider RTD curve (*i.e.* more dispersion and farther from PFR) than the RTD of the corresponding CSTRs-in-series model. This analysis also suggests that mixing in each chamber could not be solely explained by the series of ideal CSTRs.

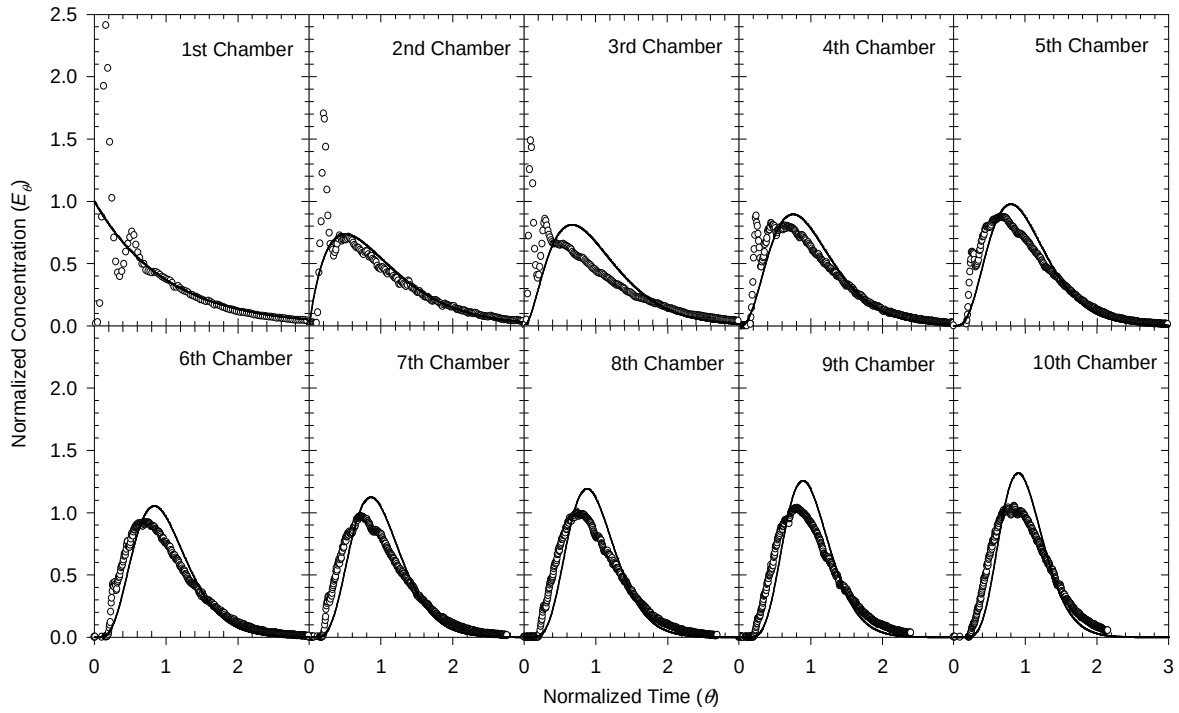

Figure 4. Normalized RTDs for different portions of the model reactor (from the inlet to the outlet of *n*th chamber, n = 1 to 10) and a corresponding model simulation for a series of n CSTRs.

In other words, if each chamber had been completely mixed using a mechanical mixer close to the theoretical maximum, the overall reactor hydrodynamics would have been closer to plug flow than the current design, which would be preferred for pathogen inactivation. Alternatively, the reactor with the same level of mixing could have been constructed using seven to eight completely mixed chambers. This non-preferred mixing characteristics resulted from the combined effect of various non-ideal flow behaviors including extensive short-circuiting from one chamber to the next through a relatively narrow baffle gap, presence of a large internal recirculation that contributes to backmixing, and the presence of a dead zone in the center of each chamber. All these flow behaviors were visually confirmed in this study using 3DLIF.

3.2 Effect of Operating Condition and Reactor Configuration

A set of experiments was performed by changing the flow rate from 12 to 18 L/min (corresponding to 45 to 69 MGD in full-scale). Analysis of the 3DLIF results (across the reactor) and normalized overall RTD curves suggested that there was no appreciable affect of flow rate on mixing for this ozone contactor.

A relatively narrow flow path through the baffle gap from one chamber to the next could be responsible for the preferential flow and short-circuiting. Experiments were performed varying the baffle gap from the original design (Figure 1a; 11 mm for overflow and 30 mm for underflow) to a wide gap condition (22mm and 60 mm, corresponding to twice the dimensions of the base-line condition) and a narrow gap condition (5.5mm and 15 mm, corresponding to half the dimensions of the base-line condition) at the same flow rate. The dimensions of 11 and 30 mm correspond to 0.46 and 1.22 m for the full-scale reactor in the LWPOF. The normalized RTD curves for a few representative chambers obtained from 3DLIF experiments are presented in Figure 5. The RTD curves obtained with varying baffle gaps were nearly identical, suggesting that the effect of baffle gap on mixing within the chamber is negligible for the range investigated.

The 3DLIF images shown in Figure 6 explain the flow patterns. When the baffle gap was narrow

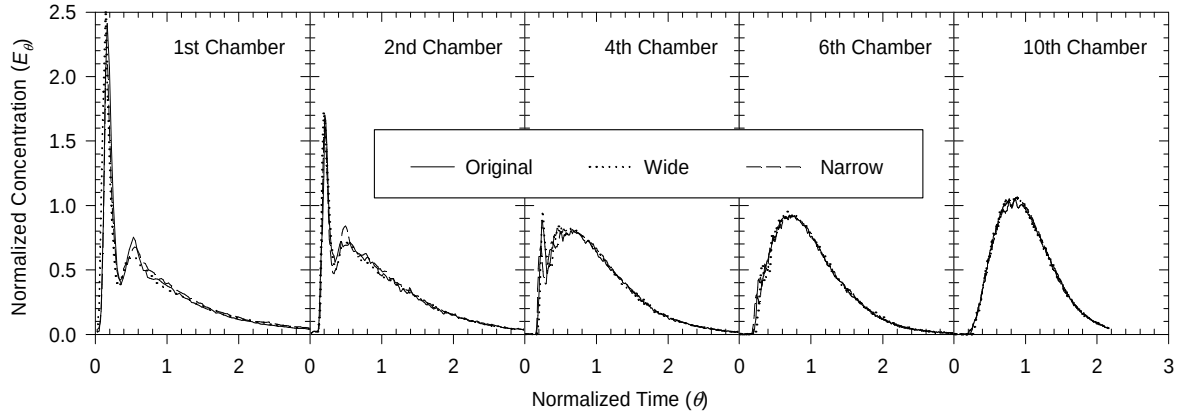

Figure 5. Normalized RTDs obtained from 3DLIF experiments performed with the model reactor with varying baffle gaps.

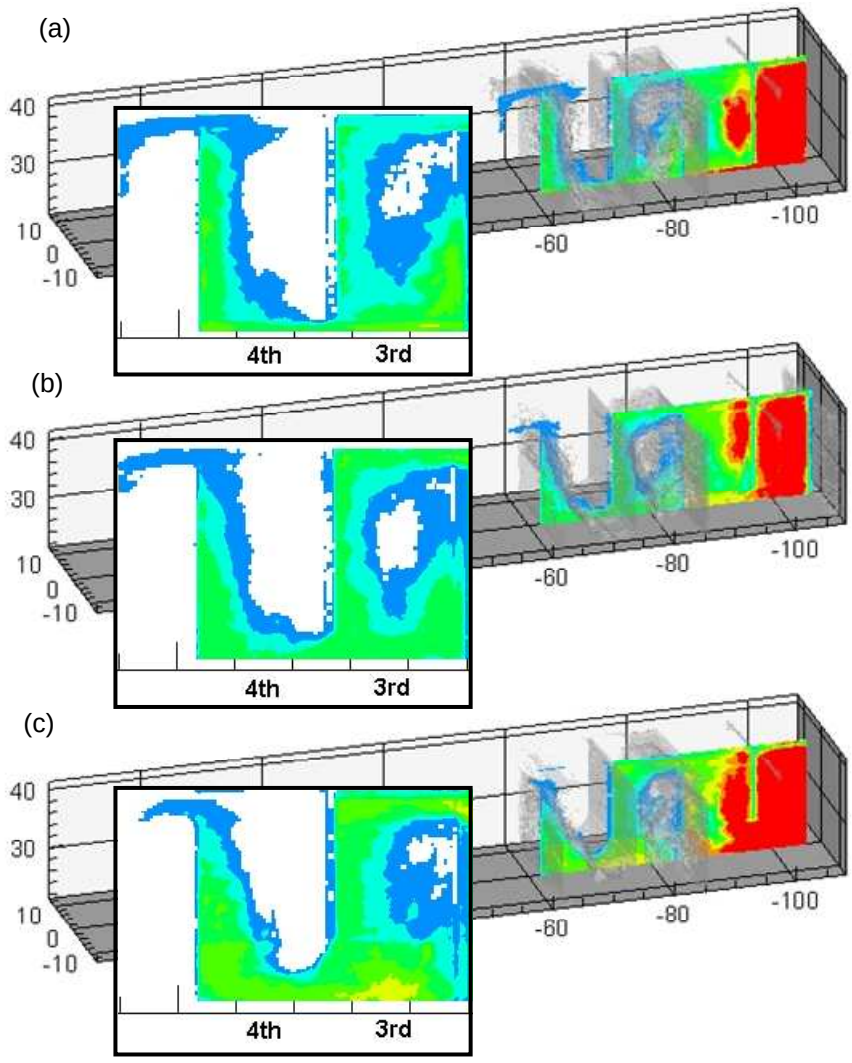

Figure 6. LIF images showing tracer dye transport through chambers with different baffle gaps: (a) narrow, (b) normal, and (c) wide baffle gaps. The images were taken 180 s after the pulse injection of the tracer.

or normal, the flow from the preceding chamber entered the subsequent reactor as a jet, which gradually expanded toward the opposing wall and flowed upward along it, resulting in short-circuiting. When the baffle gap was wide, the flow did not expand from the baffle tip, but instead initially contracted until its width was approximately one third of the channel width; it then expanded following similar to the other cases. As a result, a similar level of short-circuiting was

observed even when the baffle gap was widened four times from narrow to wide. A statistical analysis of the tracer concentration over the cross-section of the chamber outlets was performed by computing the coefficient of variation COV), defined as:

$$COV = \frac{\sqrt{\frac{1}{n-1}\times\sum_{i,j}\left(C(x,y_i,z_j,t)-\frac{1}{n}\times\sum_{i,j}C(x,y_i,z_j,t)\right)^2}}{\frac{1}{n}\times\sum_{i,j}C(x,y_i,z_j,t)} \quad (4)$$

where n is the number of data samples at a given time (= 6,200), t = time, C = the dye concentration, and i and j = indices of elements in y and z directions, respectively. The COV values (not shown) were almost identical suggesting similar mixing characteristics for these cases.

Another design variable that could affect short-circuiting is the channel width. The two-chamber reactor (Figure 1b) was run at varying chamber widths from 30 to 150 mm. The 3DLIF experimental results are shown in Figure 7. When the channel width was 150 mm (wider than the original) extensive short-circuiting and clockwise recirculation back to the chamber were observed. When the channel width was reduced to 90 and 60 mm, short-circuiting persisted (results for 60 mm not shown). However, when the channel width was reduced further to 30 mm, the tracer concentration appeared to be uniform over the chamber cross-section, and there was no indication of preferential flow.

The normalized RTD curves for the chambers with various widths are presented in Figure 8. The RTD curves also indicate the occurrence of short-circuiting in chambers wider than 60 mm (an early peak observed at $\theta < 0.5$) as well as a recirculation peak (the secondary peak at $\theta = 2$ for 120 mm-wide chamber, and at $\theta = 1$ for the 150 mm chamber). Even though the RTD curve obtained for the 30 mm wide chamber was relatively symmetrical without any apparent flow irregularity, it did not match well with CSTR-in-series model. Therefore, the RTD was fit to the ADR model with closed vessel boundary conditions (Levenspiel, 1999). The model was solved

using a finite element method (Mariñas et al. 1993) and fit to the experimental data to obtain best-fit dispersion number (*d*) of 0.26.

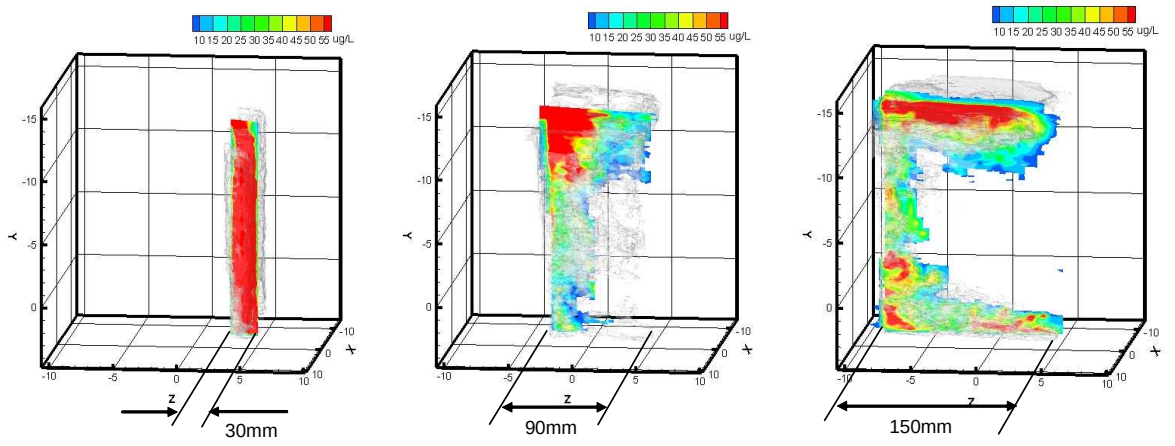

(a) (b) (c)

Figure 7. LIF images showing tracer dye transport through chambers with different channel width: (a) 30 mm, (b) 90 mm, and (c) 150 mm, taken 2.9, 5.7, and 7.4 sec, respectively, after the pulse injection of the tracer.

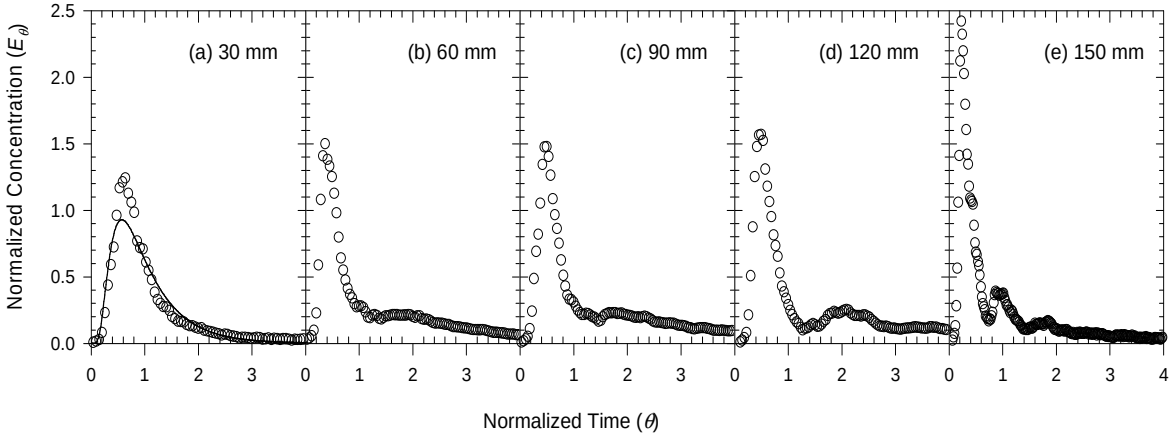

Figure 8. Normalized RTDs obtained from 3DLIF experiments performed with the model reactor with varying channel widths.

Additional reactor simulations were performed using the *Ozone Contactor Model* (*OCM*) software developed by Kim et al. (2007b). They predicted that the full-scale LWPOF ozone contactor operated at 7^{o}C would achieve a *Cryptosporidium parvum* oocyst inactivation level of approximately at 1.07 logs (91.5%). Note again that this simulation had been performed assuming the entire reactor as a series of ADRs with d = 10,000 for each chamber, the value arbitrarily chosen to designate each chamber close to an individual CSTR. If the channel width of the reactive chambers (*i.e*. the second to fourth and sixth to twelfth chambers) was reduced from the original design value of 4.8 m (120 mm in the model) to 1.2 m (30 mm for which d = 0.26 from Figure 8a) by placing additional baffle walls, the entire reactor would consist of 42 chambers. Note that the first and fifth chambers (*i.e*. transfer chambers) had different channel widths from the reactive chambers in the original design and they were not modified in the present calculation. In the revised design, the residence time of each reactive chamber would be reduced by a factor of four, while the overall residence time through the entire reactor would remain the same (neglecting the volume of additional baffle walls). The simulations were performed using the same operating conditions and the kinetic information used by Kim et al. (2007b) except that a dispersion number of 0.26 was assumed for all chambers.

The simulation results suggest that the reactor with reduced channel width could achieve the overall *C. parvum* oocyst inactivation as high as 1.20 log (93.7 %) at 7^{o}C, which is 0.13 log higher than that of the current design. It is noteworthy that this is similar to 1.23 log predicted by Kim et al. (2007b) for the LWPOF reactor operating at a near PFR condition (d = 0.01). This level is, therefore, considered fairly close to the theoretical maximum level of *C. parvum* oocyst inactivation achievable with the LWPOF reactor operating under ideal flow conditions. More importantly, the same level of inactivation (*i.e*. 1.07 log in the original design) would be achieved by reducing the total reactor volume from 0.957 MG to 0.721 MG. This corresponds to a 25% reduction in the reactor volume or a reduction of the number of chambers from 42 to 31, which would considerably reduce the construction costs. Note that decreasing the reactor volume would also reduce bromate formation from 4.0 µg/L to 3.7 µg/L. Similar calculations for 20^{o}C suggest that an additional 0.35 log inactivation (from 1.83 log to 2.18 log) can be achieved by increasing the number of baffles. Note that changing the flow condition has a greater impact at

high temperature than lower, as discussed by Kim *et al*. (2007b). When the same inactivation efficiency of 1.83 log is targeted, the contactor volume can be reduced from 0.957 MG to 0.468 MG (a 51 % reduction), which is also accompanied by a 12 % reduction in bromate formation, from 7.7 to 6.8 µg/L. This practice highlights the importance of baffle configuration to prevent the non-ideal mixing behaviors that were observed in the multi-chamber ozone contactors.

4. CONCLUSIONS

This study applied 3DLIF techniques for the first time to visualize and quantitatively investigate mixing in a multi-chamber ozone contactor, the most widely used design for water disinfection. The 3DLIF was applied to a model reactor that was scaled down from a full-scale plant currently in service. It successfully visualized the transient mixing behaviors within the contactor, which have previously been regarded as a black box in traditional tracer tests. The RTDs obtained from the model were consistent with those from the full-scale reactor. Additional experiments were performed at different flow rates, baffle gaps, and channel widths. The followings conclusions were drawn:

- The hydrodynamics in the multi-chamber reactor were characterized by extensive short-circuiting from one chamber to the next, a large internal recirculation within the chamber, and a dead zone with little mixing in the center of each chamber.
- These non-ideal mixing conditions were not affected by the flow rate and baffle gap within the range investigated.
- Reducing the channel width prevented these flow irregularities.
- Reactive transport model simulation using the *OCM* software suggested that these non-ideal mixing conditions strongly affected the overall reactor performance.
- The reactor performance could be significantly enhanced by reducing the baffle gap (by adding additional baffles) and rendering the flow through each chamber closer to a plug flow.

These findings could be useful for new plant designs as well as retrofitting existing reactors. The experimental technique is also expected to be useful for different disinfection reactors types, including chlorine contactors and UV reactors, that we are currently studying.

5. REFERENCES

Cockx, A., Do-Quang, Z., Liné, A. and Roustan, M. (1999) Use of computational fluid dynamics for simulating hydrodynamics and mass transfer in industrial ozonation towers. Chemical Engineering Science 54(21), 5085-5090.

Do-Quang, Z., Cockx, A. and Laine, J. M. (1999) Innovative design for enhanced Cryptosporidium removal in a 60 MGD WTP : Use of CFD modelling and full-scale data., Proceedings, Water Quality Technology Conference, AWWA, Tampa, FL

Do-Quang, Z., Ramirez, C.C. and Roustan, M. (2000a) Influence of geometrical characteristics and operating conditions on the effectiveness of ozone contacting in fine-bubbles conventional diffusion reactors. Ozone: Science & Engineering 22(4), 369-378.

Do-Quang, Z., Roustan, M. and Duguet, J.P. (2000b) Mathematical modeling of theoretical Cryptosporidium inactivation in full-scale ozonation reactors. Ozone: Science & Engineering 22(1), 99-111.

Hannoun, I.A. and Boulos, P.F. (1997) Optimizing distribution storage water quality: A hydrodynamic approach. Applied Mathematical Modelling 21(8), 495-502.

Hannoun, I.A., Boulos, P.F. and List, E.J. (1998) Using hydraulic modeling to optimize contact time. Journal American Water Works Association 90(8), 77-87.

Heathcote, G.R. and Drage, B.E. (1995) Development of an ozone disinfection contactor using a physical scale-model. Ozone: Science & Engineering 17(1), 15-24.

Henry, D.J. and Freeman, E.M. (1995) Finite element analysis and T-10 optimization of ozone contactors. Ozone: Science & Engineering 17(6), 587-606.

Kim, D.I., Nemlioglu, S., Roberts, P.J.W., and Kim, J.H. (2008) Ozone contactor flow visualization and quantification using three-dimensional laser-induced fluorescence. Journal American Water Works Association. (submitted).

Kim, D.I., Hasan, S., Tang, G., Mariñas, B.J., Couillard, L., Shijkairy, H. and Kim, J.H. (2007b) Simultaneous simulation of pathogen inactivation and bromate formation in full-scale ozone contactors by computer software. Journal American Water Works Association 99(8), 77-91.

Kim, J.H., Elovitz, M.S., von Gunten, U., Shukairy, H.M. and Mariñas, B.J. (2007a) Modeling Cryptosporidium parvum oocyst inactivation and bromate in a flow-through ozone contactor treating natural water. Water Research 41(2), 467-475.

Levenspiel, O. (1999) Chemical Reaction Engineering: 3th ed., John Wiley & Sons, Inc.

Munson, B.R., Young, D.F. and Okiishi, T.H. (1998) Fundamentals of fluid mechanics. 4th Edition, John. Wiley.

Murrer, J., Gunstead, J. and Lo, S. (1995) The development of an ozone contact tank simulation model. Ozone: Science & Engineering 17(6), 607-617.

Potier, O., Leclerc, J.P. and Pons, M.N. (2005) Influence of geometrical and operational parameters on the axial dispersion in an aerated channel reactor. Water Research 39(18), 4454-4462.

Rossman, L.A. and Grayman, W.M. (1999) Scale-model studies of mixing in drinking water storage tanks. ASCE: Journal of Environmental Engineering 125(8), 755-761.

Roustan, M., Beck, C., Wable, O., Duguet, J.P. and Mallevialle, J. (1993) Modeling hydraulics of ozone contactors. Ozone: Science & Engineering 15(3), 213-226.

Tang, G., Adu-Sarkodie, K., Kim, D., Kim, J.H., Teefy, S., Shukairy, H.M. and Mariñas, B.J. (2005) Modeling Cryptosporidium parvum oocyst inactivation and bromate formation in a full-scale ozone contactor. Environmental Science & Technology 39(23), 9343-9350.

Tian, X.D. and Roberts, P.J.W. (2003) A 3D LIF system for turbulent buoyant jet flows. Experiments in Fluids 35(6), 636-647.

USEPA (1991) Guidance manual for compliance with the filtration and disinfection requirements for public water systems using surface water sources. USEPA, Washington.

Villermaux, J. (1982) Génie de la réaction chimique conception et fonctionnement des réacteurs, Tec&Doc. Lavoisier, Paris.

APPENDIX

Additional data that was collected during the project is presented herein. This data revealed compelling new directions for further research, but the breadth of experiments was not sufficient to establish any conclusions that could be a part of the final report.

Reactive Tracer Test. We have performed a reactive tracer test with the goal of visualizing and quantitatively analyzing the distribution of *CT* (*i.e.* concentration of ozone in a semi-batch reactor and contact time) inside the model multi chamber ozone contactor used in this study. In brief, the feed water contains a fixed amount of reactive tracer which decays due to the reaction with ozone that is introduced into the inlet of the reactor. Therefore, the region of the reactor with less dye would indicate the region with higher ozone exposure or *CT*. By correlating the intensity of the fluorescence (hence the concentration of dye) with *CT*, the *CT* distribution within the reactor is quantitatively analyzed.

Carboxylated fluorescence microspheres (0.05 µm Fluoresbrite yellow-orange, Polyscience, Warrington, PA) was used as a reactive tracer. Preliminary tests performed with Rhodamine 6G and microspheres with different sizes (1.0 and 0.2 µm) suggested that they were not appropriate for this purpose due to too rapid kinetics (*i.e.* degradation by ozone) and turbidity, respectively. In order to obtain calibration between fluorescence intensity and *CT*, microspheres were ozonated in a semi-batch reactor for a specified contact time at 1.0 mg O_3/L. After the reaction was completed, the remaining dissolved ozone was instantaneously quenched using 0.1 mL of 0.1 M sodium thiosulfate solution. The ozonated solution was then placed in a rectangular acrylic container (5 mm W $\times$ 25 mm H $\times$ 28 mm L). A planar laser was beamed into the container and fluorescence image was obtained. After processing the image using *TFlook* software, the fluorescence intensities over the entire image were averaged pixel by pixel. The obtained fluorescence value was linearly correlated with corresponding *CT*. For the flow-through experiments, the dechlorinated tap water (500 L) containing the microspheres was fed to the model reactor at the flow rate of 6 L/min. An ozone stock solution (12.3 mg O_3/L) was injected

into the reactor inlet at a flow rate of 0.26 L/min to achieve target ozone concentration at the reactor inlet as 0.5 mg/L. The 3DLIF images were obtained as discussed above.

Figure A1 shows the experimental results obtained with the reactive tracer test. Figure A1(a) shows the spatial distribution of fluorescence in the first six chambers of the model ozone contactor. This image was further processed pixel-by-pixel using the following relationships obtained from the semi-batch calibration experiments,

$$CT = \frac{55.1 - F}{0.60} \qquad \text{for } 20 \le F \le 55 \text{ (} F \text{ = fluorescence intensity in each pixel)}$$

$$CT = \frac{24.7 - F}{0.07} \qquad \text{for } 0 \le F \le 20$$

to obtain Figure A1(b) which shows the distribution of *CT* within the reactor. It is noticeable that the *CT* gradually increases as water flows through the reactor (*i.e*. color changing from blue to red). A closer look at the second chamber suggests that *CT* would be higher in the middle of the chamber, in which dead zone forms, while it would be lower in the peripheral region in which flow short-circuits. Although the results reasonably well reflect the expected behavior and does provide a quantitative information on *CT* distribution within the ozone contactor for the first time in literature, a relatively large level of data noise was also noticeable especially when *CT* was relatively high. This resulted, as fluorescence intensity became very low when microspheres were extensively ozonated. Nevertheless, the results suggest that further study is required to establish a more defined experimental protocol for reactive tracer tests to obtain accurate *CT* distribution within the contactor. Understanding such a distribution is expected to provide valuable information on reactor performance diagnosis and a highly effective tool for reactor design.

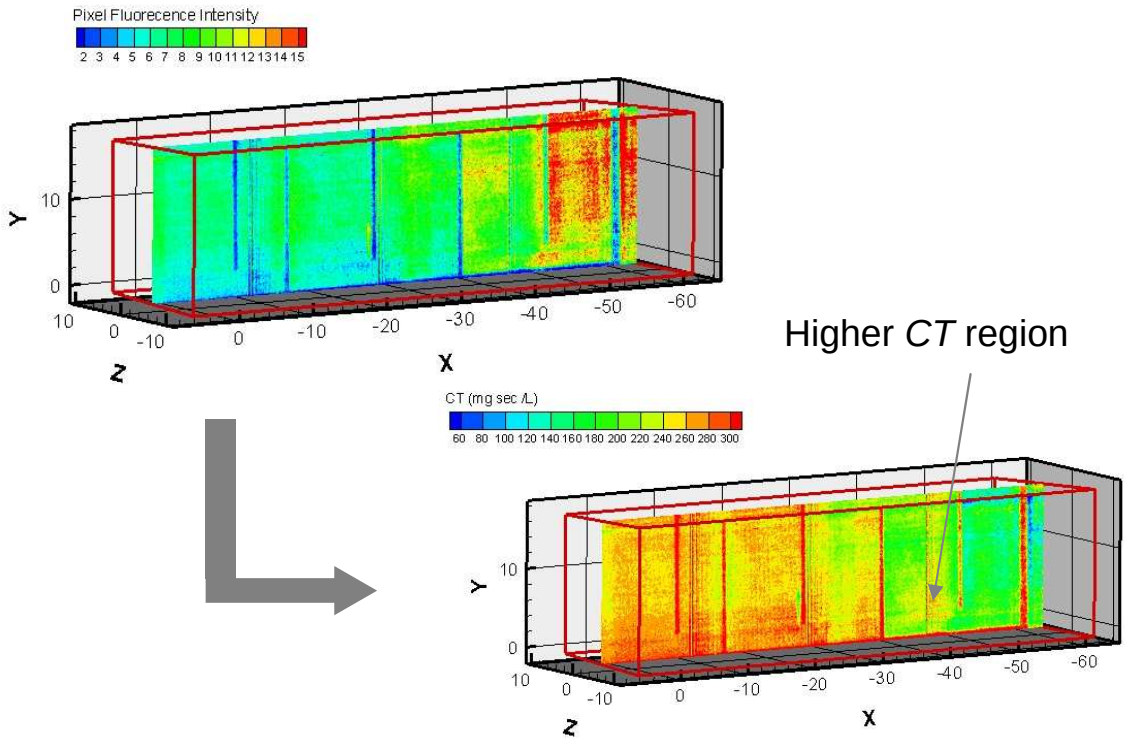

Figure A1. Spatial distribution of fluorescence intensity (upper) and *CT* (lower) in the model ozone contactor obtained from reactive tracer test performed with 3DLIF system.